Journal of Power Sources 196 (2011) 7025–7029

Contents lists available at ScienceDirect

Journal of Power Sources

journal homepage: www.elsevier.com/locate/jpowsour

Short communication

High capacity and high rate capability of nanostructured $CuFeO_2$ anode materials for lithium-ion batteries

Lin Lu[a], Jia-Zhao Wang[a,b,*], Xue-Bin Zhu[a,c], Xuan-Wen Gao[a], Hua-Kun Liu[a,b]

[a] Institute for Superconducting and Electronic Materials, University of Wollongong, NSW 2522, Australia
[b] ARC Centre of Excellence for Electromaterials Science, University of Wollongong, NSW 2522, Australia
[c] Key Laboratory of Materials Physics, Institute of Solid State Physics, Chinese Academy of Sciences, Hefei 230031, People's Republic of China

ARTICLE INFO

Article history:
Received 12 August 2010
Received in revised form
28 September 2010
Accepted 29 September 2010
Available online 7 October 2010

Keywords:
$CuFeO_2$
Anode
Li-ion battery
Charge/discharge
Capacity

ABSTRACT

Non-toxic, cheap, nanostructured ternary transition metal oxide $CuFeO_2$ was synthesised using a simple sol–gel method at different temperatures. The effects of the processing temperature on the particle size and electrochemical performance of the nanostructured $CuFeO_2$ were investigated. The electrochemical results show that the sample synthesised at 650 °C shows the best cycling performance, retaining a specific capacity of 475 mAh g^{-1} beyond 100 cycles, with a capacity fading of less than 0.33% per cycle. The electrode also exhibits good rate capability in the range of 0.5*C*–4*C*. At the high rate of 4*C*, the reversible capacity of $CuFeO_2$ is around 170 mAh g^{-1}. It is believed that the ternary transition metal oxide $CuFeO_2$ is quite acceptable compared with other high performance nanostructured anode materials.

1. Introduction

Rechargeable Li batteries offer the highest energy density of any battery technology, and they power most of today's portable electronics. One of the most attractive applications for lithium batteries is to power electric vehicles (EV) and hybrid electric vehicles (HEVs). However, for EV/HEV applications, the rechargeable battery requires high energy density, high power, and high rate capability. The current techniques for producing rechargeable lithium batteries have difficulty in satisfying all these requirements. In the last decade, great efforts have been devoted to the development of various new electrode materials to meet the requirements for large batteries [1–3].

Nanostructured transition metal oxides are attractive materials as prospective anodes to replace graphite in lithium-ion batteries (LIBs) due to the high reversible capacities [1,4]. Nanostructured binary transition metal oxides, such as Co_3O_4, NiO, Fe_2O_3, and Cu_2O, have been extensively studied [5–8]. They demonstrate high theoretical capacities, but have poor cycle life due to large volume expansion and contraction during the Li^+ insertion and extraction reactions [9]. Recently, nanostructured ternary transition metal oxides have been explored as anode materials to improve cyclability [10–13]. Chowdari's group has reported that galvanostatic cycling of $CuCo_2O_4$ at 60 mA g^{-1} in the voltage range of 0.005–3.0 V vs. Li metal exhibits only a small capacity fading of 2 mAh g^{-1} per cycle for up to 50 cycles [10]. Compared with $CuCo_2O_4$, $CuFeO_2$ is more desirable for use as anode material, as it is much cheaper and non-toxic. $CuFeO_2$ is one of the stable compositions in the Cu–Fe–O ternary system, and was historically the first known compound exhibiting the so-called delafossite structure [14–16]. Analogous to $CuCo_2O_4$ [10], the reaction of the nanostructure $CuFeO_2$ with Li can be represented by Eqs. (1)–(3). The reversible capacity can be expected to correspond to 4 mol of Li per mole of $CuFeO_2$ (Eqs. (2) and (3)):

$$CuFeO_2 + 4Li^+ + 4e^- \rightarrow Cu + Fe + 2Li_2O \quad (1)$$

$$2Cu + Li_2O \leftrightarrow Cu_2O + 2Li^+ + 2e^- \quad (2)$$

$$2Fe + 3Li_2O \leftrightarrow Fe_2O_3 + 6Li^+ + 6e^- \quad (3)$$

Sukeshini's group has reported that lithium can intercalate into $CuFeO_2$ at a voltage of about 1 V vs. Li/Li^+ [12]. However, the cyclability and high rate capability of $CuFeO_2$ anode materials for lithium-ion batteries have never been investigated. Therefore, we synthesised nanostructured $CuFeO_2$ using a simple sol–gel method. This technique does not require any high cost precursors and produces powders with particle sizes less than 1 μm. The cycle life and the high rate capability of nanostructured $CuFeO_2$ have been studied in detail for the first time.

* Corresponding author at: Institute for Superconducting and Electronic Materials, University of Wollongong, AIIM Facility, Innovation Campus, Squires Way, Fairy Meadow, NSW 2519, Australia. Tel.: +61 2 4298 1478; fax: +61 2 42215731.
E-mail address: jiazhao@uow.edu.au (J.-Z. Wang).

0378-7753/$ – see front matter © 2010 Elsevier B.V. All rights reserved.
doi:10.1016/j.jpowsour.2010.09.108

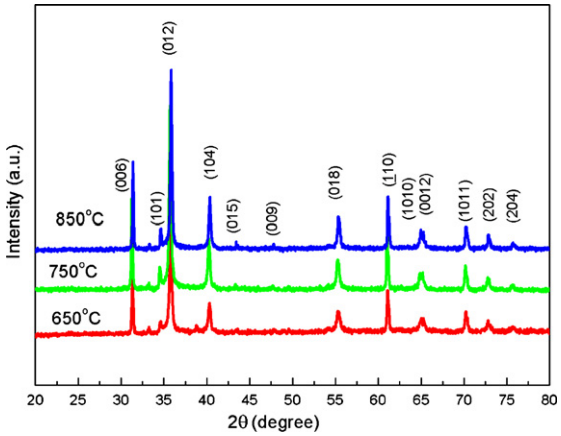

Fig. 1. X-ray diffraction patterns of $CuFeO_2$ powders prepared at different temperatures.

2. Experimental

Nanostructured $CuFeO_2$ powders were prepared by the sol–gel method at different temperatures. All the precursors were obtained from Sigma–Aldrich and directly used as received. 0.025 M $Cu(NO_3)_2{\cdot}2.5H_2O$ (99.99%) and 0.025 M $Fe(NO_3)_3{\cdot}9H_2O$ (98 + %) were dissolved in 40 ml ethylene glycol and stirred at room temperature for more than 10 h in order to achieve a well-mixed solution. Then, the solution was dried to a powder at 65 °C in a vacuum oven. The powder was ground in an agate mortar and baked at 300 °C under argon atmosphere for 10 h to expel the organics. Finally, the baked powder was crystallized at temperatures in the range of 650–850 °C under argon atmosphere for 10 h. The structural and morphological properties of the derived samples were investigated by X-ray diffraction (XRD) with Cu Kα radiation and field-emission scanning electron microscopy (FESEM; JEOL 7500 at 5 kV).

The electrochemical characterizations were carried out using 2032 coin cells. The electrodes were prepared by dispersing 70 wt.% $CuFeO_2$ as the active material, 20 wt.% acetylene carbon black, and 10 wt.% CMC binder in distilled water to form homogeneous slurry. The slurry was spread onto pieces of copper foil. The electrodes were dried at 100 °C in a vacuum oven overnight and then pressed to enhance the contact between the active material and the conductive carbon. The cells were assembled using lithium metal foil as the counter electrode in an argon-filled glove box. The electrolyte solution was 1 M $LiPF_6$ in ethylene carbonate:diethyl carbonate (EC:DEC) at 1:2 (v/v). Constant-current charge–discharge tests were performed in the range of 3.00–0.01 V vs. Li/Li^+ using a Land battery tester at different current densities. Cyclic voltammetry (CV) was carried out using a CHI 660C electrochemical workstation between 0.01 V and 3.0 V at a scanning rate of 0.1 mV s^{-1}.

3. Results and discussion

3.1. Structural and morphological characterization

The XRD patterns of the $CuFeO_2$ samples are shown in Fig. 1. The characteristic peaks of all $CuFeO_2$ samples correspond well with standard crystallographic data (JCPDS-No 00-039-0246). The crystal structure belongs to the space group $R3m$ with $a = 3.0347$ Å, $c = 17.162$ Å in the hexagonal description. The structure consists of hexagonal layers of Cu, O, and Fe with a stacking sequence of A-B-C along the c-axis to form a layered triangular lattice antiferromagnet, where the triangular lattices of magnetic Fe^{3+} are separated by non-magnetic ion layers of Cu^+ and O^{2-} [16]. The average crystallite size of the $CuFeO_2$ powders was determined by using Traces® software and the Scherrer formula. The crystallite sizes are 38, 48, and 54 nm for the samples prepared at 650 °C, 750 °C, and 850 °C, respectively.

The particle sizes and morphologies of the samples synthesised at three temperatures, as revealed by FESEM images, are shown in Fig. 2. The sizes of the particles are in range of 100–300 nm, 300–500 nm, and 800–1000 nm for the 650 °C, 750 °C, and 850 °C samples, respectively. The particle sizes obviously became larger with increasing temperature. It can be clearly observed that all samples consist of particles with fairly narrow size distributions and cubic morphologies.

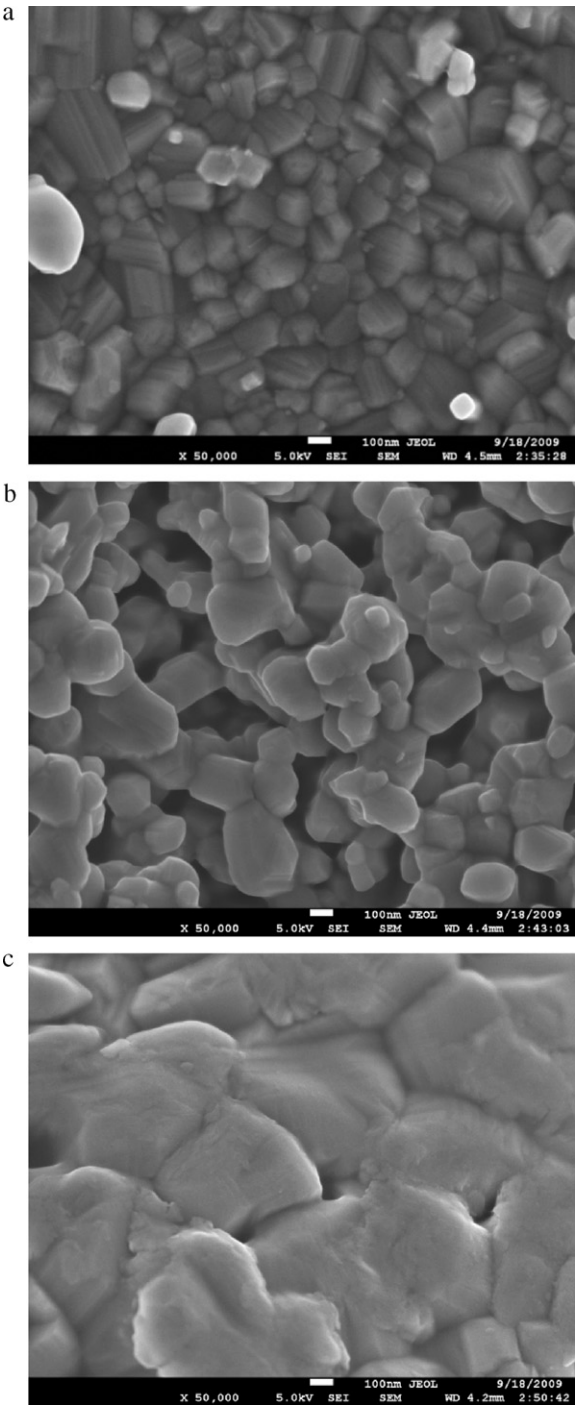

Fig. 2. FE-SEM images of $CuFeO_2$ powders: (a) 650 °C, (b) 750 °C and (c) 850 °C.

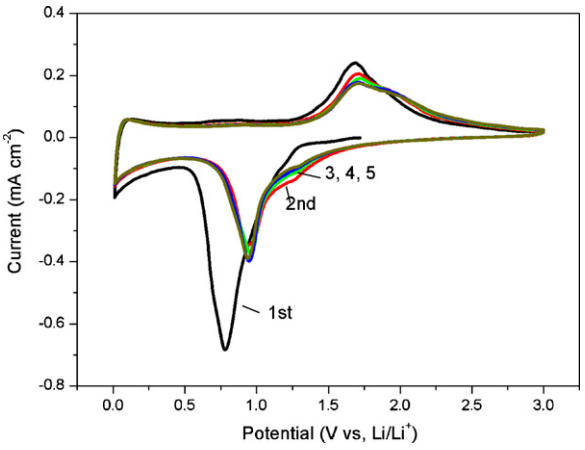

Fig. 3. Cyclic voltammetry of $CuFeO_2$ electrode with the powders prepared at 650 °C.

3.2. Cyclic voltammetry and reaction mechanism

It has been reported that the transition metal oxides are electrochemically inactive in bulk form, but they have electrochemical activity in nanoscale form because the mechanism of Li reactivity differs from classical Li insertion/extraction or Li-alloying process [17,18]. Therefore, nanostructured $CuFeO_2$ was synthesised in this study. The electrochemical properties were investigated to confirm the reactivity of $CuFeO_2$ in the lithium cell.

In order to investigate the electrochemical properties of the $CuFeO_2$ materials as anode for lithium-ion batteries, cyclic voltammetry (CV) and charge/discharge testing were used for the measurement of the batteries. Fig. 3 shows the CV curves of an electrode containing $CuFeO_2$ powder prepared at 650 °C. The CV of the first discharge reaction has a broad peak at 0.79 V with an onset at 1.25 V. The peak in the first discharge cycle is attributable to decomposition of the $CuFeO_2$ structure and formation of Cu and Fe nanoparticles in an amorphous matrix of Li_2O (Eq. (1)), as well as to formation of the solid electrolyte interphase (SEI) [19,20]. The first discharge reaction is an irreversible process that destroys the structure. One broad peak around 1.4–2.2 V in the charge cycle can be assigned to the oxidation of both the Cu and the Fe metal nanoparticles to their respective metal oxides of Cu_2O and Fe_2O_3 (forward reactions of Eqs. (2) and (3)), as well as to the decomposition of the SEI [8,19,20].

The second and subsequent discharge sweeps are characterised by two cathodic peaks at 0.95 V and 1.3 V, are attributed to the reduction of Cu_2O, Fe_2O_3, Li^+ and the formation of the SEI [8,19,20]. The relatively higher voltage of 0.95 V in comparison to the 0.79 V observed in the first discharge CV curve indicates that the reaction mechanism with Li differs from the first discharge reaction and represents the formation of Cu and Fe from the respective oxides, Cu_2O and Fe_2O_3, according to the backward reactions of Eqs. (2) and (3). There is an anodic peak at 1.7 V with a shoulder in the range of 1.85–1.95 V in the second and subsequent charge sweeps. The anodic peak with shoulder corresponds to the reversible oxidation of Fe^0, Cu^0, and Li_2O to produce Fe_2O_3, Cu_2O, and Li^+ ions [20,21]. From the second cycle onward, the reversible reaction takes place as given by Eqs. (2) and (3).

3.3. Galvanostatic cycling

Charge–discharge cycling was performed in the half-cell configuration with $CuFeO_2$ as cathode vs. Li-metal in the voltage range of 0.01–3.0 V at a current density of 100 mA g^{-1}. Fig. 4 presents the discharge–charge curves for the $CuFeO_2$ electrode prepared at 650 °C. The first discharge profile indicates that the working voltage falls rapidly from the open potential to 1.15 V, and then a long voltage plateau in the range of 1.15–0.75 V is followed by a sloping curve to the cut-off voltage of 0.01 V, which is consistent with the CV of the first discharge curve. $CuFeO_2$ is decomposed to electrochemical active Cu and Fe, while Li_2O is also formed in this process (Eq. (1)). The overall first discharge capacity is about 935 mAh g^{-1}, which is higher than the theoretical first discharge capacity of 708 mAh g^{-1}. The extra capacity results from the formation of the SEI at the electrode/electrolyte interface during the first discharge process [5]. The first charge profile shows a smoothly varying curve followed by a plateau at 1.7 V. The nanoparticles of Cu and Fe undergo an oxidation reaction, which converts them to Cu_2O and Fe_2O_3 during this process, according to the forward reactions of Eqs. (2) and (3). The overall first charge capacity is 718 mAh g^{-1}, which is 23% lower than the first discharge capacity, a discrepancy which is attributed to the incomplete decomposition of Li_2O and the SEI [21].

The second discharge profile is different from that of the first discharge, indicating the different reaction mechanism, which also corresponds well with the CV studies. The second discharge curve is smooth, with a slightly higher voltage plateau at 1.1 V, followed by a sloping curve to 0.01 V. The metal oxides, Cu_2O and Fe_2O_3, react with Li^+ and are converted to nanosize Cu and Fe particles (Eqs. (2) and (3)). The overall second discharge capacity is 704 mAh g^{-1}, which is very close to the first charge capacity (718 mAh g^{-1}) and the theoretical discharge capacity of 708 mAh g^{-1}. This shows that the electrochemical reaction is almost completely reversible.

The voltage profiles of other selected cycles are also shown in Fig. 4. These voltage profiles are similar to the second cycle profile, which indicates good lithium recyclability after the first cycle. The gradually decreasing spread of the voltage profiles reveals the continuous capacity fading upon cycling. The voltage plateau indicates that the formation of Cu and Fe metal particles occurs at 1.1 V, while the distribution of the charge capacity is over the whole charge cycle with an average charge potential of 1.7 V. This indirectly suggests that the average reaction voltages involving Cu and Fe are almost the same, due to the metal-ion and Li_2O matrix effects [10].

Fig. 5 displays the cycling performances of the $CuFeO_2$ electrodes synthesised at different temperatures, 650 °C, 750 °C, and 850 °C. The particle sizes are 100–300 nm, 300–500 nm, and 800–1000 nm for the samples prepared at 650 °C, 750 °C, and 850 °C, respectively. All samples exhibited large reversible capacities during the initial 5 cycles, and then the capacities gradually decreased. The first discharge capacities are 935 mAh g^{-1}, 992 mAh g^{-1}, and 1007 mAh g^{-1} for the $CuFeO_2$ electrodes prepared at 650 °C, 750 °C, and 850 °C, respectively. Subsequently, the

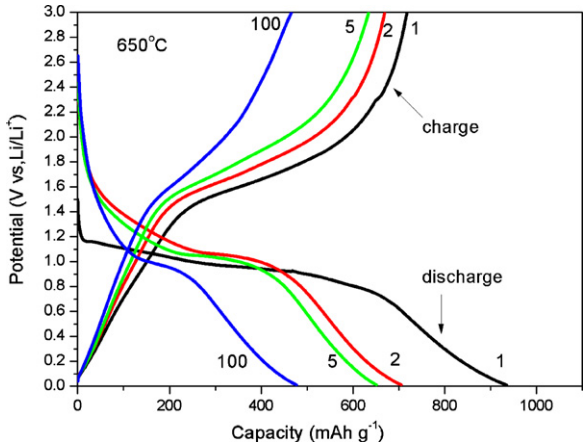

Fig. 4. Typical charge–discharge curves of $CuFeO_2$ electrode with the powders prepared at 650 °C.

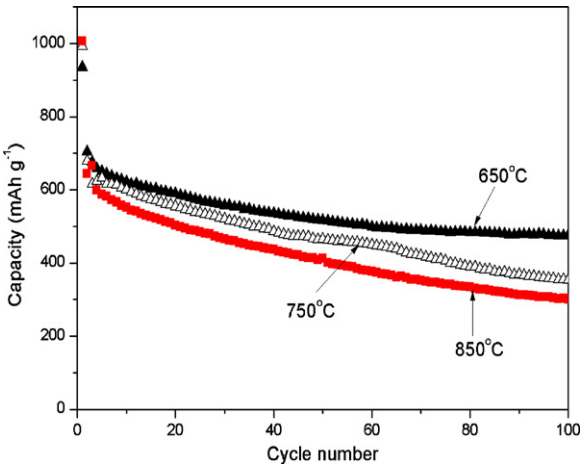

Fig. 5. Cycling performances of $CuFeO_2$ electrodes with the powders prepared at 650 °C, 750 °C and 850 °C, respectively.

discharge capacities beyond 100 cycles were maintained at 475, 353, and 300 mAh g^{-1}, and the capacity retention compared to the second cycle capacity was 67.5%, 52%, and 46.6%, for the $CuFeO_2$ electrodes prepared at 650 °C, 750 °C, and 850 °C, respectively. The results revealed that the capacities are increased when the particle sizes are reduced. The sample with smallest particle size, which was prepared at 650 °C, showed the best capacity retention. The good electrochemical performances of the sample with the smallest particle size may be due to the following reasons:

(1) The proportion of the total number of atoms that lie near or on the surface is increased when the particle size is reduced. Therefore, the available electroactive surface area is increased, resulting in enhanced electrochemical reactivity [1,22].
(2) Small particles can more easily accommodate the structural strains due to the lithium insertion than large ones, resulting in excellent capacity retention [23].

3.4. Rate capability

For the application of lithium-ion batteries to hybrid electric vehicles, good rate capability is necessary for the electrode materials. The observed high and stable capacity of $CuFeO_2$ samples encouraged a study of the rate capability using various current densities at ambient temperature. The rate capability test was conducted on the powder prepared at 650 °C. The specific current was increased in several steps after every 20 cycles from 0.5*C* to 4*C*. Fig. 6 shows the discharge capacity under different current densities in the range from 0.5*C* to 4*C* (1*C* = 708 mA g^{-1}). After the current density was increased in a stepwise fashion, it was then decreased in two steps at 0.5*C* and 0.25*C*. The capacity values decrease with increasing current rate, as can be expected. At the high rate of 4*C* (discharge/charge of all active materials within 15 min, i.e., 2832 mA g^{-1}), the reversible capacity of $CuFeO_2$ is around 170 mAh g^{-1}. The results are quite acceptable in comparison with other high performance nanostructured anode materials [24]. When the current rate was decreased from 4*C* to 0.5*C*, the capacity increased to 405 mAh g^{-1}, and the recovery was 77% of the value at 0.5*C*. When the current rate was further decreased to 0.25*C*, the capacity reached 506 mAh g^{-1}, which is equal to the retained capacity for the same $CuFeO_2$ electrode when cycled at 0.14*C* (100 mA g^{-1}) over 55 cycles, as shown in Fig. 5. The results showed that $CuFeO_2$ exhibits good rate-dependent behaviour and quite stable capacity at each current density.

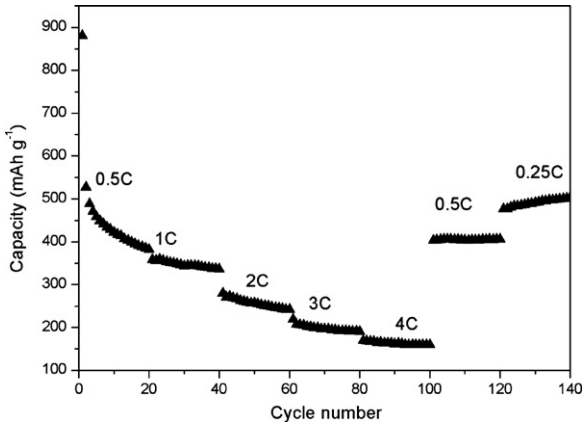

Fig. 6. Capacity vs. cycle number plot at various current rates of nanocrystalline $CuFeO_2$ electrodes. The *C* values corresponding to different current rates are indicated, assuming 1*C* = 708 mA g^{-1}.

4. Conclusion

$CuFeO_2$ powders were prepared by the simple sol–gel method at different temperatures (650 °C, 750 °C, and 850 °C). FESEM images showed higher synthesis temperatures yielding relatively larger particle sizes. The particle size has a significant effect on the electrochemical performance. The sample prepared at 650 °C exhibited the highest capacity retention of 67.5% of the second cycle value up to the 100th cycle at 100 mA g^{-1}, and also showed an acceptable result at the high rate of 4*C*. The results confirmed that the nanostructured ternary transition metal oxide $CuFeO_2$ is a promising anode material for the lithium-ion batteries.

Acknowledgements

Financial support provided by the Australian Research Council through an ARC Discovery Project (DP 0987805) and ARC Centre of Excellence funding is gratefully acknowledged. Technical assistance on the SEM measurements provided by Mr. Darren Attard is highly appreciated. Many thanks also go to Dr. T. Silver for critical reading of the manuscript.

References

[1] P. Poizot, S. Laruelle, S. Grugeon, L. Dupont, J.M. Tarascon, Nature 407 (2000) 496.
[2] A.K. Padhi, K.S. Nanjundaswamy, J.B. Goodenough, J. Electrochem. Soc. 144 (1997) 1188.
[3] A.D.W. Todd, R.E. Mar, J.R. Dahn, J. Electrochem. Soc. 154 (6) (2007) A597–A604.
[4] K.F. Zhoug, X. Xia, B. Zhang, H. Li, Z.X. Wang, L.Q. Chen, J. Power Sources 195 (2010) 3300–3308.
[5] S.L. Chou, J.Z. Wang, H.K. Liu, S.X. Dou, J. Power Sources 182 (2008) 359–364.
[6] X.H. Huang, J.P. Tu, X.H. Xia, X.L. Wang, J.Y. Xiang, Electrochem. Commun. 10 (9) (2008) 1288–1290.
[7] J. Chen, L. Xu, W.Y. Li, X.L. Gou, Adv. Mater. 17 (2005) 582–586.
[8] J.Y. Xiang, J.P. Tu, Y.F. Yuan, X.H. Huang, Y. Zhou, L. Zhang, Electrochem. Commun. 11 (2009) 262–265.
[9] X.B. Zhu, S.L. Chou, L. Wang, Q. Li, D.Q. Shi, J.Z. Wang, Z.X. Chen, Y.P. Sun, H.K. Liu, S.X. Dou, Electrochem. Solid-State Lett. 12 (9) (2009) A176–A180.
[10] Y. Sharma, N. Sharma, G.V. Subba Rao, B.V.R. Chowdari, J. Power Sources 173 (2007) 495–501.
[11] Y Sharma, N. Sharma, G.V. Subba Rao, B.V.R. Chowdari, Electrochim. Acta 53 (2008) 2380–2385.
[12] A.M. Sukeshini, H. Kobayashi, M. Tabuchi, H. Kageyama, Solid State Ionics 128 (2000) 33–41.
[13] X.J. Zhu, L.M. Geng, F.Q. Zhang, Y.X. Liu, L.B. Cheng, J. Power Sources 189 (1) (2009) 828–831.
[14] E.M. Levin, C.R. Robbins, H.F. McMuride, Phase Diagrams for Ceramists, American Ceramic Society, Columbus, OH, 1964, p. 53.
[15] P. Dordor, J.P. Chaminade, A. Wichainchai, E. Marquestaut, J.P. Doumerc, M. Pouehard, P. Hagenmuller, J. Solid State Chem. 75 (1988) 105.
[16] A. Pabst, Am. Mineral. 31 (1946) 539.
[17] C. Jiang, E. Hosono, H. Zhou, Nanotoday 1 (4) (2006) 28.

[18] M.M. Rahman, J.Z. Wang, X.L. Deng, Y. Li, H.K. Liu, Electrochim. Acta 55 (2009) 504–510.
[19] H. Liu, G.X. Wang, J. Park, J.Z. Wang, H.K. Liu, C. Zhang, Electrochim. Acta 54 (2009) 1733–1736.
[20] C.Q. Zhang, J.P. Tu, X.H. Huang, Y.F. Yuan, X.T. Chen, F. Mao, J. Alloys Compd. 441 (2007) 52–56.
[21] Z.M. Cui, L.Y. Jiang, W.G. Song, Y.G. Guo, Chem. Mater. 21 (2009) 1162–1166.
[22] J. Chen, J.Z. Wang, G. Wallace, A.I. Minett, Y. Liu, C. Lynam, H.K. Liu, Energy Environ. Sci. 2 (2009) 393–396.
[23] D. Larcher, C. Masquelier, D. Bonnin, Y. Chabre, V. Masson, J.B. Leriche, J.M. Tarascon, J. Electrochem. Soc. 150 (2003) pA133.
[24] Y.M. Kang, K.T. Kim, K.Y. Lee, S.J. Lee, J.H. Jung, J.Y. Lee, J. Electrochem. Soc. 150 (2003) A1538.